engineering proceedings

MDPI

Proceeding Paper

Static Mechanical Property Criterion Determined under Different Extent of Hot Crack Index of High-Strength Aluminium Autogenous Laser Welds †

François Nadeau * and Fatemeh Mirakhorli

National Research Council of Canada, 501 Boulevard Université Est, Saguenay, QC G7H 8C3, Canada; fatemeh.mirakhorli@cnrc-nrc.gc.ca

* Correspondence: francois.nadeau@cnrc-nrc.gc.ca

† Presented at the 15th International Aluminium Conference, Québec, QC, Canada, 11–13 October 2023.

Abstract: Nowadays, vehicle electrification is growing at a fast pace due to stringent environmental regulations on carbon emissions in North America. The manufacturing of E-mobility battery components such as enclosures evolves at the same trend and many new design concepts are put in place. As health and safety in electric vehicles are taken very seriously by OEMs, the enclosures are still heavy but are likely to become more lightweight in years to come, using high-strength aluminium alloys as one of the potential solutions, as weight directly affects the admissible range. In this paper, four (4) different aluminium wrought alloys (AA6061, AA6010, AA7020 S and AA7075) were autogenously laser-welded using various parameters and inspected through 2D X-ray tomography. A hot crack index (HCI), using optical microscopy, was defined in order to quantify the internal extent of hot cracks. Static mechanical butt joint tensile tests were provided to dictate a mechanical property criterion regarding the extent of HCI. This revealed that uniform elongation is a good predictor of the extent of HCI in terms of static mechanical behavior. These findings could eventually be used to define a threshold value toward a safe number of hot cracks in laser welds.

Keywords: high-strength aluminium; laser welding; hot cracking

Citation: Nadeau, F.; Mirakhorli, F. Static Mechanical Property Criterion Determined under Different Extent of Hot Crack Index of High-Strength Aluminium Autogenous Laser Welds. *Eng. Proc.* **2023**, *43*, 11. https://doi.org/10.3390/engproc2023043011

Academic Editor: Mario Fafard

Published: 13 September 2023

1. Introduction

Automakers are undergoing a transformational change by embracing the electrification of vehicles (EV) on a large scale. The new design solutions must surpass consumer demands and sustainability priorities while keeping a competitive edge. In addition, the part and material selection need to meet each individual engineering requirements depend on the application, and in this regard, aluminium is one of the fastest-growing materials in the mix. According to the Aluminium Association, high-strength aluminium alloys, especially the AA6xxx and AA7xxx series, will be pushed forward in the short- (1–5 years) and mid-term (5–10 years), allowing for thickness reduction in manufactured components which will ultimately improve light-weighting [1]. This light-weighting is foreseen by automotive manufacturers as they expect a high growth of EVs in the SUV and pickup sectors, as the batteries are larger and require longer range. Aluminium battery enclosures are generally complex structures including a structural frame, a cooling system and top and lower covers combining extrusions, sheets and castings [2]. On the joining side, different techniques have been demonstrated, such as friction stir welding (FSW) and adhesive bonding, but laser welding is also gaining ground as it allows a very high productivity throughput [3–5]. Laser welding can be used in its autogenous variant, meaning without using a filler wire, or wire-assisted, which refers to the laser cold-wire (LCW) variant. LCW, as it introduces a filler wire, achieves generally lower travel speeds when compared to the autogenous variant [6]. For this reason, autogenous laser welding in fillet and overlap joint configurations is an interesting approach toward production. Nonetheless, some hurdles are expected relative to aluminium battery enclosure laser welding applications, including leak-proof and crack-free welds. The hot cracking susceptibility of aluminium welds has been extensively studied, but it is still a performance criterion to consider. The alloy composition plays a major role and the AA6xxx and AA7xxx series are more susceptible to hot cracking due to the addition of magnesium, silicon, copper and zinc chemical elements [7–9]. Some researchers have published on the hot cracking behavior of autogenous laser welds. Holzer et al. presented a relative hot crack length index value, which is defined as the cumulative crack length measured in the fusion zone divided by the weld length, on 2.0 mm thick AA7075 butt laser welds [10,11]. The hot cracks were not visible from the metallographic transverse cut sections and the hot crack index evaluation was performed over the sub-surface and longitudinal cut sections where most of the cracks appeared. This showed hot crack index values ≤0.5 at travel speeds between 2.0 and 10.0 m/min and relatively low laser power (2.8 kW) using a nominal spot diameter of 200 µm. However, their micrographs suggest some amount of underfill at the surface and bottom of the welds due to their small spot diameter. The ultimate tensile strength was provided, but without extensive details on the obtained stress–strain curves and elongation at fracture values. The fusion zone microstructure in laser welds is also an important factor toward hot cracking. Hagenlocher et al. showed a reduction in hot cracking susceptibility by increasing the number of grain boundaries across the width of the weld in AlMgSi aluminium alloys [12]. This behavior can be achieved by reducing the laser weld parameters (laser power and travel speed), which resulted in a reduction of the grain size or an enlargement of the width of the fusion zone with an equiaxed grain microstructure. In addition, the laser wobbling welding variant has seen wider adoption with regard to joining aluminium alloys in the last few years. This variant, under oscillation of the laser beam, promotes the formation of finer equiaxed grains in the fusion zone as well as an improvement in the overall weld quality with lower porosity content and heat input [13,14].

In this study, wobbling laser welding variants under high-power lasers (≥5.5 kW) and travel speeds (≥4.5 m/min) were developed in overlap and butt joint configurations over different aluminium alloys (AA6061, AA6010, AA7020 S and AA7075) and parameters in order to correlate the hot crack index (HCI) with their respective stress–strain curve-extracted criteria (yield stress, ultimate tensile stress, elongation at fracture). These results allowed the definition of a potential threshold hot crack index limit value on the acceptance of autogenous wobbling laser welds subjected to static loadings.

2. Materials and Methods

The aluminium alloys evaluated are provided in Table 1 with regard to their chemical composition.

Table 1. Experimental chemical compositions of the aluminium alloys.

Alloy	Al	Mg	Si	Cu	Zn	Fe	Mn	Cr
AA6061	Bal.	1.11	0.70	0.29	0.11	0.53	0.11	0.19
AA6010 [1]	Bal.	0.80	0.93	0.23	0.17	0.31	0.54	0.01
AA7020 S [1]	Bal.	1.09	0.03	0.00	3.92	0.13	0.15	0.12
AA70705	Bal.	2.31	0.07	1.37	5.68	0.15	0.03	0.20

[1] Sheets supplier: Speira.

The chemical composition was obtained using optical emission spectroscopy (OES). The aluminium sheets were of 2.0 mm thickness, except for the AA6010 alloy, which was provided in 4.0 mm thicknesses. The sheets were then machined down with a CNC Haas machine to a 2.0 mm final thickness prior to laser welding. The laser welding experiments were conducted under various metallurgical processing routes (Table 2).

Table 2. Metallurgical state processing route of laser welds for a given aluminium alloy.

Al Alloy	Metallurgical State Processing Route of Laser Welds
AA6061	T6 → Laser weld (T4)
AA6010	F → Laser weld (T4) → Artificial aging (T6) [1]
AA7020 S	F → Solution heat treatment and artificial aging (T6) → Laser weld (T4) [1]
AA7075	T6 → Laser weld (T4)

[1] Solution heat treatment and artificial aging procedure is kept proprietary (achieving peak aging).

As this study was conducted under a METALTec industrial group umbrella at NRC, the industrial members imposed specific initial and final metallurgical state drive by a potential application. The autogenous welds were realized using a Trumpf TruDisk 10 kW laser source coupled with a Precitec YW52 processing laser wobbling head and integrated on a Fanuc M800iA 60 kg payload robot (Figure 1).

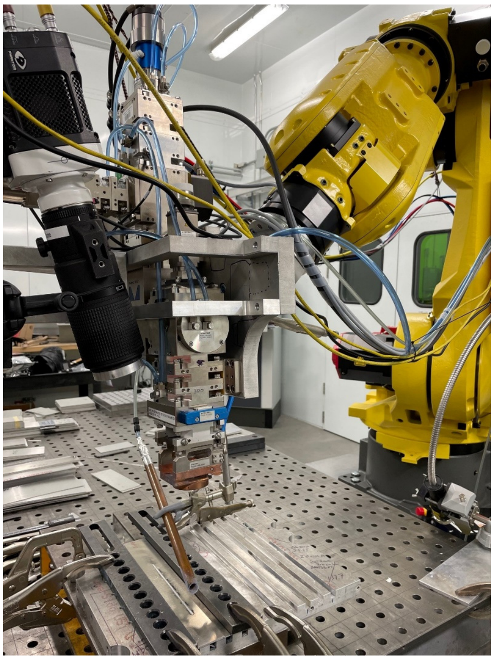

Figure 1. Trumpf TruDisk 10 kW laser source coupled with a YW52 Precitec wobbling laser processing head integrated on a Fanuc M800iA 60 kg payload robot.

A laser beam analysis was conducted at 1 kW power using a PRIMES system (Figure 2).

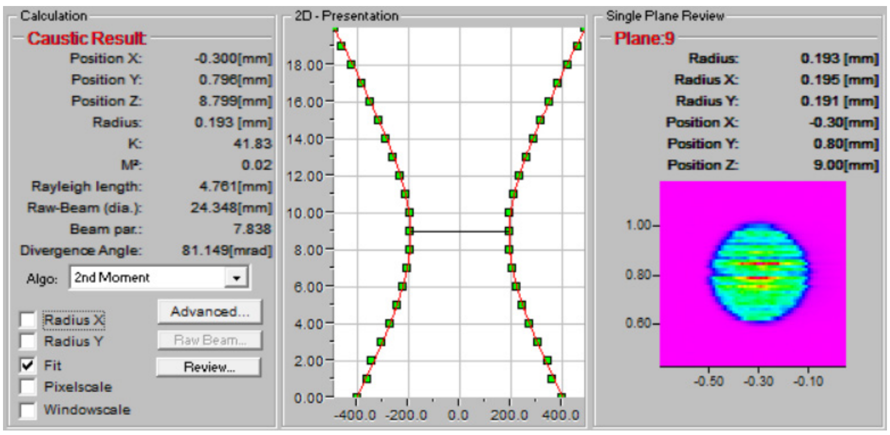

Figure 2. PRIMES beam analysis at 1 kW on the YW52 Precitec wobbling laser processing head showing the beam characteristic at focal plane.

The PRIMES results show a laser spot diameter of 386 µm at the focal plane by a combination of a 150 mm collimator and 300 mm focal lens sizes. All the laser welding trials were performed at the focal plane position of +10 mm above the material, which gave a focal spot size of 920 µm based on the PRIMES analysis. The sheet dimensions were of at least 150 mm in width and 300 mm in length and were shear-cut. The clamping system allowed minimal gaps prior to laser welding. At first, autogenous laser welds were performed in overlap joint configurations where the material being studied for hot cracking was positioned as the top sheet (Figure 3).

Figure 3. Overlap laser joint configuration.

The main laser weld parameters are provided in Table 3.

Table 3. Autogenous wobbling laser overlap welding parameters on various alloys as top sheet.

Alloy	Laser Weld ID	Laser Power kW	Robot Speed m/min	Wobbling Amplitude mm	Wobbling Frequency Hz
AA6061	1	7.5	8.0	0.2	400
AA6061	2	7.0	7.0	1.0	400
AA6061	3	6.0	6.5	0.5	400
AA6010	1	7.0	6.5	0.5	400
AA6010	2	6.5	5.5	0.5	400
AA6010	3	6.0	5.0	0.5	400
AA7020 S	1	6.5	6.0	0.5	400
AA7020 S	2	6.0	5.0	0.8	200
AA7020 S	3	5.5	4.5	0.5	400
AA7075	1	8.0	7.0	1.5	400
AA7075	2	6.0	6.5	0.5	400
AA7075	3	5.5	5.0	0.5	400

These parameters were developed in order to reach high travel speeds (4.5–8.0 m/min). The focal distance was always set ≥10.0 mm independently of the aluminium alloy as it provided a more stable weld and a better surface finish. The laser welds were quality-controlled for internal porosity under a 2D X-ray YXLON non-destructive (NDE) inspection system calibrated with a #5 circular image quality indicator (IQI) and 2-2T sensitivity level described in ASTM E1025. Figure 4 shows the 2D X-ray NDE system and a typical analysis.

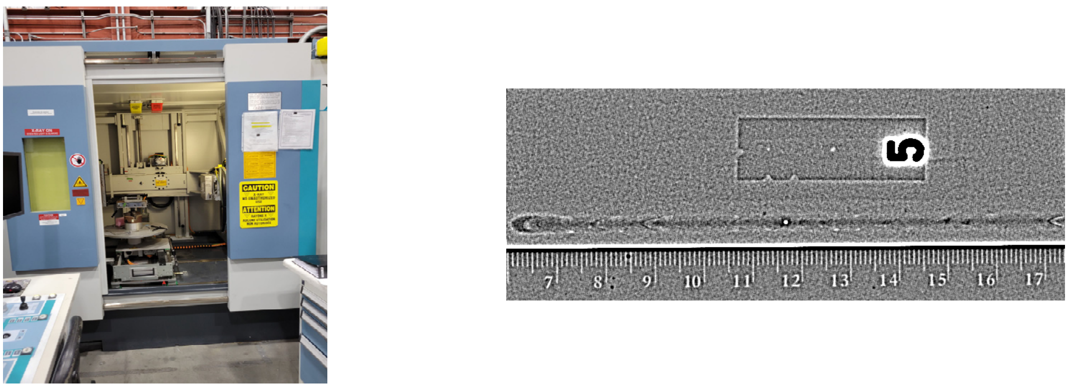

(**a**) (**b**)

Figure 4. (**a**) 2D X-ray YXLON NDE inspection system; (**b**) typical 2D X-ray analysis on laser weld using an IQI #5.

This pre-qualification acts as a preventive method on laser-welded sheets with a high number of internal porosities or visible macrocracks to be qualified further. A transverse microstructural analysis was conducted using a HF 3% etchant as a pre-weld qualification procedure in order to evaluate the overall weld quality, especially the undercut depth. A top-view microstructural analysis was also conducted without etching for the hot crack measurements. Specimen polishing was performed carefully to remove no more than 0.7 mm at the sub-surface (1/3 of weld thickness) as was previously stated by Holzer et al. [10,11]. The hot crack measurements were conducted using an Olympus optical microscope at a 100× magnification with a Clemex Vision® (https://clemex.com/) software analysis tool. An image analysis routine was developed to recognize all the large cracks adequately, as well as the microcracks independently of their respective width (Figure 5). The hot crack index was defined as the equation below:

$$Hot\ crack\ index\ (HCI) = \frac{Cumulative\ hot\ crack\ length\ (mm)}{Weld\ length\ (mm)} \quad (1)$$

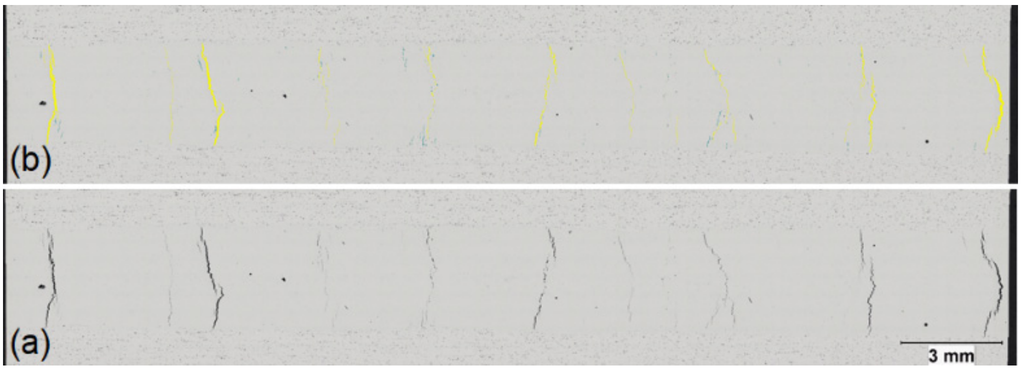

Figure 5. Microstructural analysis routine development. (**a**) as polished; (**b**) after running the Clemex Vision® routine.

A sufficient weld length was considered in the analysis, as it was observed, in some specimens, that the hot crack behavior can follow a specific pattern (repetitive larger cracks perpendicular to the weld path). The mechanical properties were obtained from tensile specimens machined from the base material and laser-welded sheets using Tensilkut® equipment following ASTM B557 subsize standard guidelines (Figure 6).

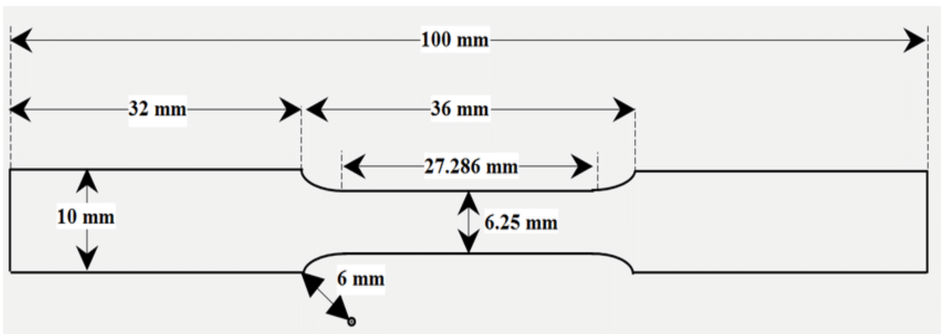

Figure 6. ASTM B557 subsize specimen dimensions.

The tensile test procedure also followed the same standard on a MTS electromechanical RT100 machine equipped with a 25 mm gage length mechanical extensometer.

3. Results and Discussion

3.1. Microstructure and Hot Crack Index Measurements

The transverse micrographs of overlap laser welds are provided in Figures 7–10 for aluminium alloys AA6061, AA6010, AA7020 S and AA7075 as the top sheet, respectively, upon different laser weld parameters. No visible microcracks were found within the transverse weld micrograph on every aluminium alloy or laser parameters, as reported in the work of Holzer et al.

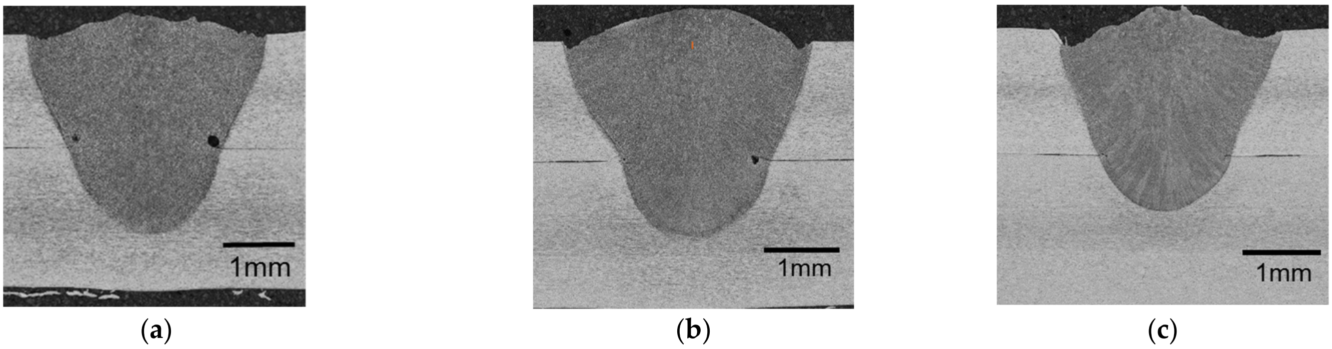

Figure 7. AA6061/AA6061 overlap laser weld transverse micrographs: (**a**) 7.5 kW, 8.0 m/min; (**b**) 7.0 kW, 7.0 m/min; (**c**) 6.0 kW, 6.5 m/min.

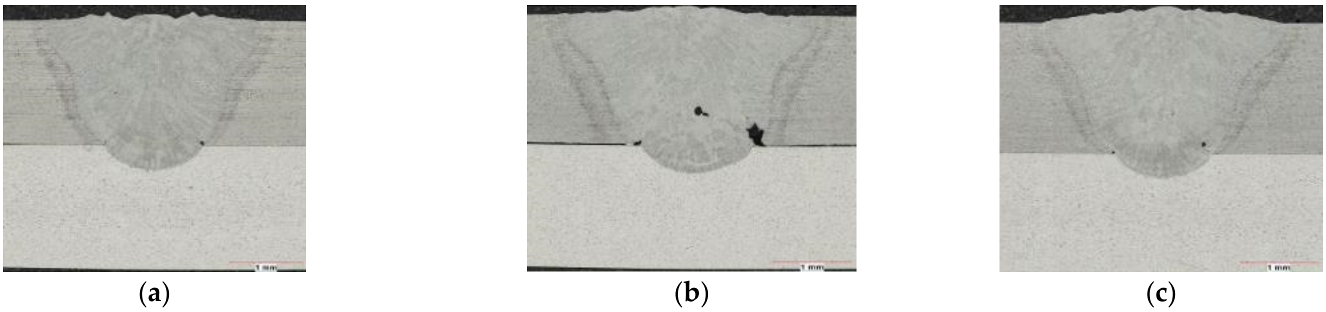

Figure 8. AA6010/AA6061 overlap laser weld transverse micrographs: (**a**) 7.0 kW, 6.5 m/min; (**b**) 6.5 kW, 5.5 m/min; (**c**) 6.0 kW, 5.0 m/min.

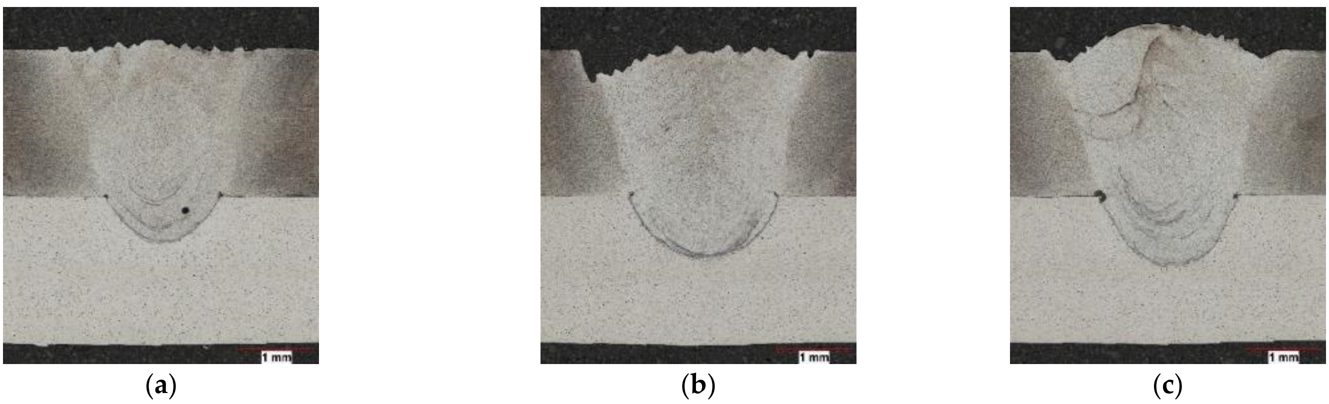

Figure 9. AA7020 S/AA6061 overlap laser weld transverse micrographs: (**a**) 6.5 kW, 6.0 m/min; (**b**) 5.5 kW, 5.0 m/min; (**c**) 5.5 kW, 4.5 m/min.

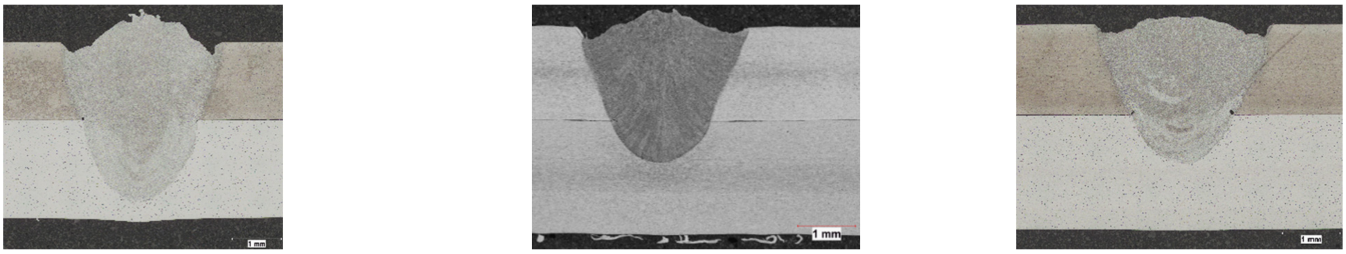

(**a**) (**b**) (**c**)

Figure 10. AA7075/AA6061 overlap laser weld transverse micrographs: (**a**) 8.0 kW, 7.0 m/min; (**b**) 6.0 kW, 6.5 m/min; (**c**) 5.5 kW, 5.0 m/min.

The underfill amount was higher on AA7xxx laser welds compared to AA6xxx ones, which was expected from the evaporation of zinc and magnesium chemical elements [15]. The fusion zone area was measured using ImageJ® software and the results are shown in Figure 11. There was no direct relationship between the fusion zone area and the laser power, nor with the aluminium alloy. However, the largest fusion zones were observed at the highest laser power (≥7.5 kW). The sub-surface top-view micrographs are provided in Figures 12–15.

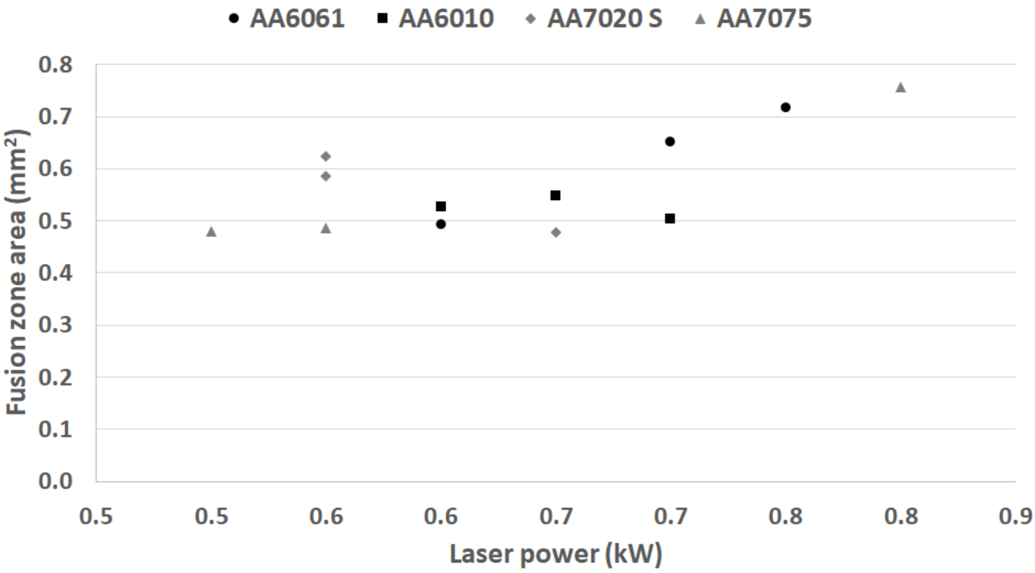

Figure 11. Fusion zone area of autogenous laser welds relative to the laser power.

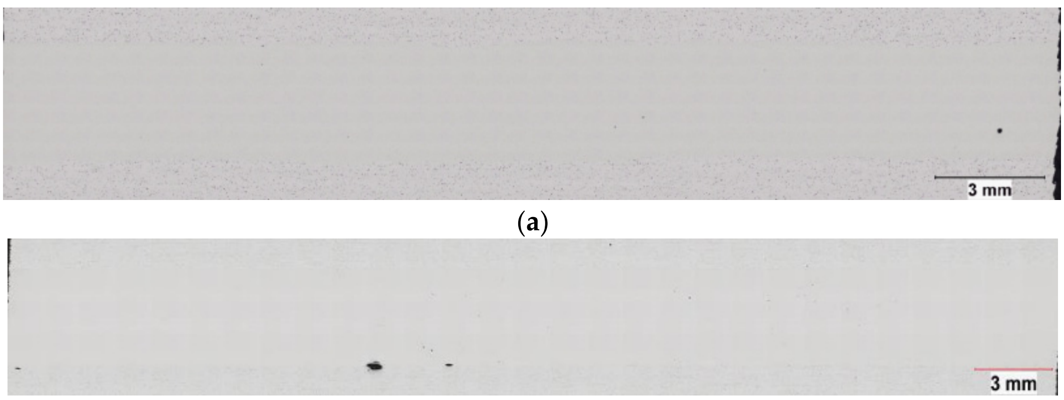

(**a**)

(**b**)

Figure 12. *Cont.*

(c)

Figure 12. Sub-surface top-view micrograph of AA6061 laser welds: (**a**) 7.5 kW, 8.0 m/min; (**b**) 7.0 kW, 7.0 m/min; (**c**) 6.0 kW, 6.5 m/min.

(a)

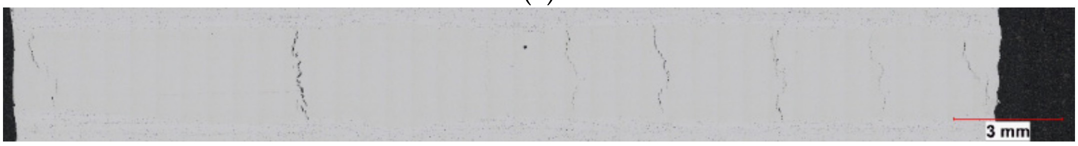

(b)

(c)

Figure 13. Sub-surface top-view micrograph of AA6010 laser welds: (**a**) 7.0 kW, 6.5 m/min; (**b**) 6.5 kW, 5.5 m/min; (**c**) 6.0 kW, 5.0 m/min.

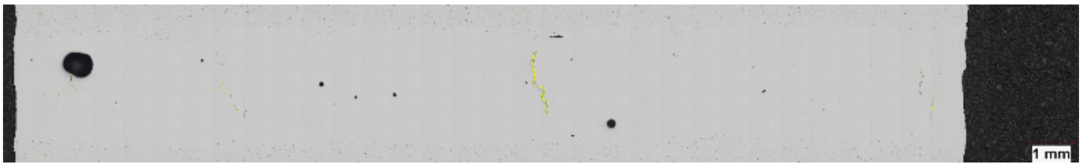

(a)

(b)

(c)

Figure 14. Sub-surface top-view micrograph of AA7020 S laser welds: (**a**) 6.5 kW, 6.0 m/min; (**b**) 5.5 kW, 5.0 m/min; (**c**) 5.5 kW, 4.5 m/min.

(**a**)

(**b**)

(**c**)

Figure 15. Sub-surface top-view micrograph of AA7075 laser welds: (**a**) 8.0 kW, 7.0 m/min; (**b**) 6.0 kW, 6.5 m/min; (**c**) 5.5 kW, 5.0 m/min.

The hot crack index was calculated for each aluminium alloy and laser parameters (Table 4) and a graphical display as function of the laser power is shown in Figure 16.

Table 4. Hot crack index (HCI) measurements on the different aluminium alloys and laser weld parameters.

Alloy	Laser Power kW	Robot Speed m/min	Total Crack Length mm	Total Weld Length mm	Hot Crack Index (HCI)
AA6061	7.5	8.0	0.00	30.1	0.00
AA6061	7.0	7.0	0.00	40.6	0.00
AA6061	6.0	6.5	6.97	30.1	0.23
AA6010	7.0	6.5	27.36	27.4	1.00
AA6010	6.5	5.5	22.74	27.5	0.83
AA6010	6.0	5.0	8.35	29.6	0.28
AA7020 S	6.5	6.0	10.54	22.9	0.46
AA7020 S	6.0	5.0	5.58	22.9	0.24
AA7020 S	5.5	4.5	5.15	21.6	0.24
AA7075	8.0	7.0	50.10	29.7	1.69
AA7075	6.0	6.5	81.00	29.6	2.74
AA7075	5.5	5.0	56.77	28.2	2.01

From these results, it can be seen that AA6061 aluminium alloy has a low number of cracks, the highest value peaking at 0.23 independently of the laser weld parameters. On the other hand, AA6010 aluminium alloy showed higher HCI values ranging from 0.28 to 1.00. An important increase in the HCI value was observed when the laser power increased from 6.0 kW to 7.0 kW, as well as in the travel speed (5.0 m/min to 6.5 m/min). It was previously stated by Zhang et al. that the addition of copper (Cu) to AA6xxx aluminium alloys (Al-Mg-Si) improves the cracking susceptibility index (CSI) [16]. Given the chemical composition of our AA6010 sheets, the CSI index could reach values between 4–5 at 0.2% Cu. Then, the HCI index appears to be a function of the chemical composition and the welding cooling rate. In comparison, AA6061 aluminium alloy shows a CSI index closer to 3–4. Referring still to that paper, it is seen that AA7075 exhibits a CSI index between 6–7 while AA7020 is between 4–5. The HCI values obtained on the AA7020 S laser welds followed a similar relationship compared to AA6010. The values increased from 0.24 to 0.46 as the laser power and travel speed increased. It is interesting to note that even if the CSI index reached 4–5 for alloys AA6010 and AA7020 S, the HCI index in laser welding could be controlled to a low value (<0.3) if the laser power was kept below 6 kW combined with a travel speed below 5.0 m/min. For AA7075, the CSI index minimal value was very high, pending at 7.5. Independently of the laser weld parameters, the HCI index was very high (≥1.69). Ultimately, the CSI index of the base material correlated quite well with the autogenous laser weld HCI values obtained in our study and highlights the effect of the laser parameters to control, to some extent, the HCI value.

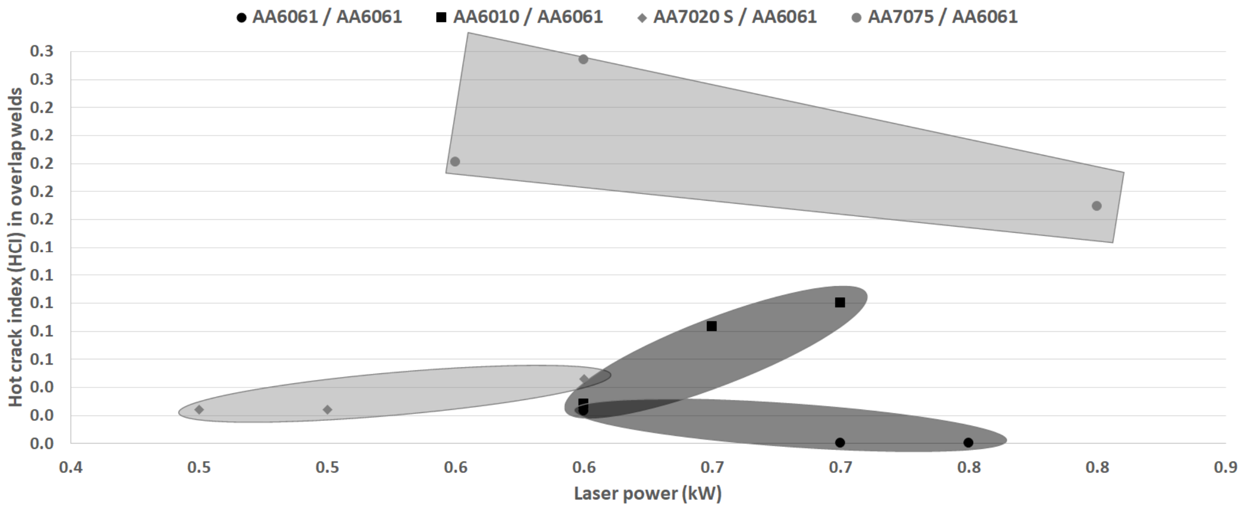

Figure 16. Hot crack index (HCI) of various aluminium alloy autogenous laser welds as function of the laser power.

A broader discretization of the hot cracks is provided in Table 5, as well in Figures 17–19, where every single crack was measured (width, length, aspect ratio). The results excluded AA6061 laser welds given the lower number of hot cracks. The hot cracks were divided into two classes relative to their length (<500 µm, ≥500 µm). For AA6010 laser welds, most of the hot cracks were long (≥500 µm) and very few small cracks (<500 µm) were found. At the lowest laser power (6.0 kW), an important decrease in the number of large cracks was observed, which resulted in the lower HCI index. For AA7020 S, the behavior was slightly different, as at the highest laser power (6.5 kW), a higher number of small cracks (<500 µm) accounted for the increase in the HCI index from 0.24 to 0.46. The AA7075 laser welds exhibited the same trend but the number of small cracks was higher in comparison with the other aluminium laser-welded alloys. Nonetheless, the number of large hot cracks (≥500 µm) increased from 16 to 26 as the laser power increased from 5.5 kW to 8.0 kW. At the same time, surprisingly, the number of small cracks decreased from 412–443 to 155.

This decrease was responsible for the lower HCI index at high laser power (8 kW) when compared to a lower laser power (5.5–6.0 kW). This behavior was only observed on the AA7075 aluminium alloy.

3.2. Mechanical Static Tensile Behavior

For mechanical testing, a butt joint laser weld configuration was preferred in order to remove the stress concentration effect at the weld interface with the overlap joint configuration.

Table 5. Hot crack measurements for various autogenous laser weld parameters of aluminium alloys AA6010, AA7020 S and AA7075.

Alloy	Laser Weld ID	Hot Crack Class	Number Count	Total Crack Length mm	Mean Crack Width µm	Mean Crack Length µm	Aspect Ratio
AA6010	1	<500 µm	4	1.09	39.1	274	7.34
		≥500 µm	20	26.27	161.8	1313	7.47
	2	<500 µm	4	1.34	38.4	336	9.15
		≥500 µm	18	22.00	150.1	1189	7.70
	3	<500 µm	1	0.33	55.2	332	6.02
		≥500 µm	4	8.02	136.7	2006	11.19
AA7020 S	1	<500 µm	8	9.26	115.4	1158	9.82
		≥500 µm	7	1.27	28.9	182	7.14
	2	<500 µm	1	3.00	14.6	2997	204.57
		≥500 µm	13	2.58	24.4	199	8.40
	3	<500 µm	2	3.92	74.8	1959	10.47
		≥500 µm	9	1.23	137.2	137	6.98
AA7075	1	<500 µm	26	37.68	177.8	1449	8.44
		≥500 µm	155	12.42	16.0	80	4.80
	2	<500 µm	22	37.04	227.2	1684	8.27
		≥500 µm	443	44.07	18.0	100	5.50
	3	<500 µm	16	25.48	197.3	1592	8.64
		≥500 µm	412	31.29	15.8	76	4.69

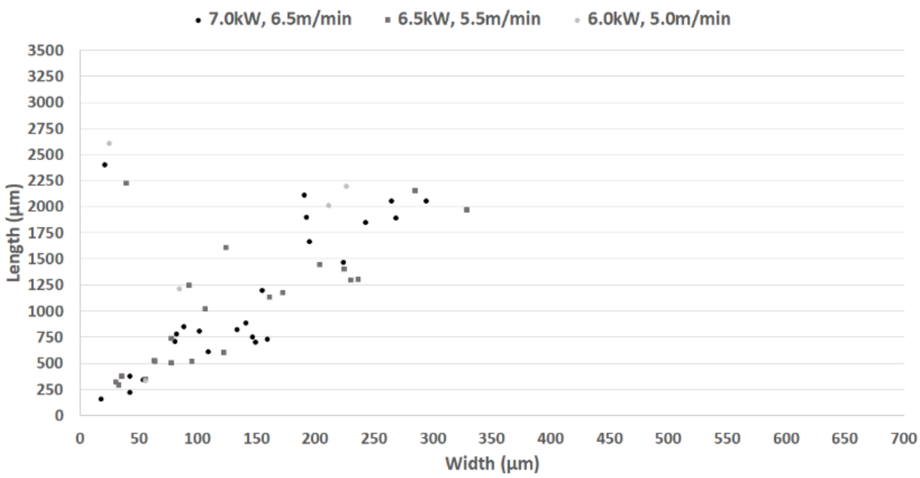

Figure 17. Length and width of hot cracks observed in AA6010 laser welds on various parameters.

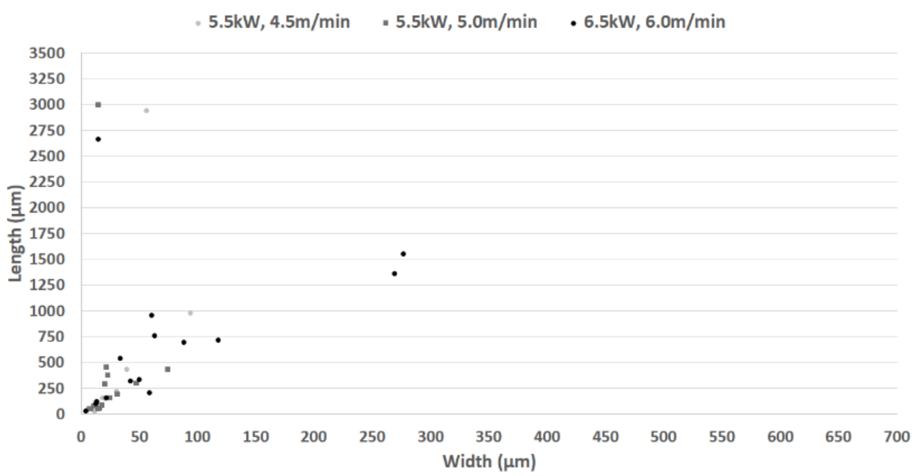

Figure 18. Length and width of hot cracks observed in AA7020 S laser welds on various parameters.

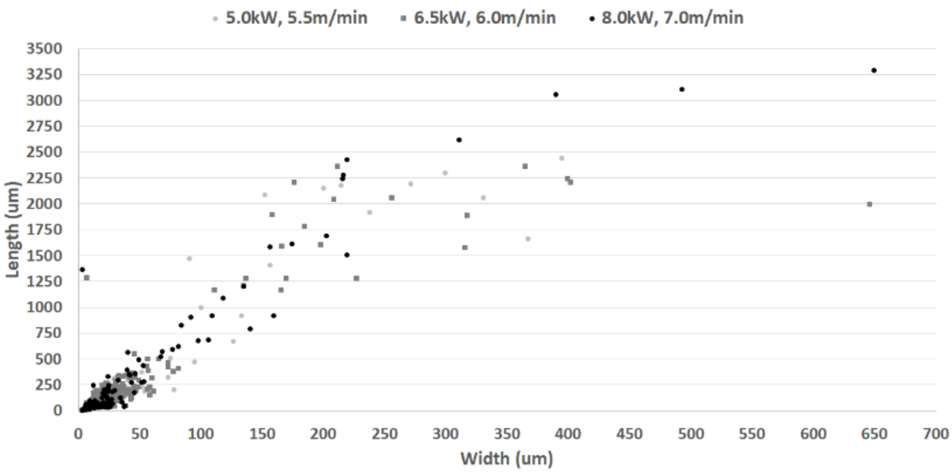

Figure 19. Length and width of hot cracks observed in AA7075 laser welds on various parameters.

This latter configuration was tested previously and the tensile stress–strain curves were similar without regard to the aluminium alloy. The welding parameters were kept constant since the required butt weld penetration was in the same range (2.0 mm). A HCI validation analysis was conducted on AA6010 and AA7075 aluminium alloys over two conditions to ensure that the values were equivalent for both overlap and butt joints (Table 6, Figure 20).

Table 6. Hot crack measurements for AA6010 and AA7075 laser butt welds; validation point.

Alloy	Laser Power kW	Robot Speed m/min	Total Crack Length mm	Total Weld Length mm	Hot Crack Index (HCI)
AA6010	6.0	5.0	8.35	29.6	0.26
AA7075	8.0	7.0	32.17	20.17	1.60

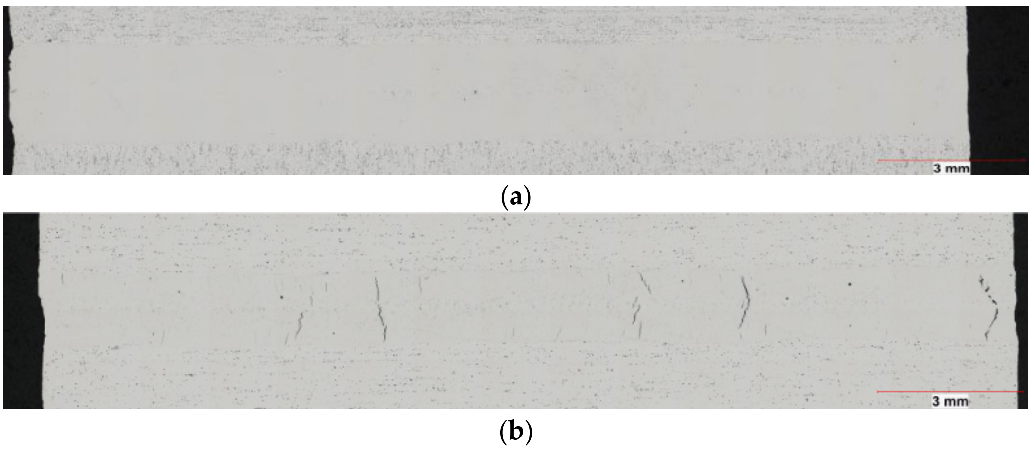

Figure 20. Sub-surface top-view micrograph of AA6010 and AA7075 laser butt welds (**a**) AA6010, 6.0 kW, 5.0 m/min; (**b**) AA7075, 8.0 kW, 7.0 m/min.

The HCI index of the butt joint welds (Table 6) are comparable to the ones obtained on the overlap welds (Table 4). The mechanical tensile curves are provided in Figure 21, comparing five different laser weld HCI indexes upon the four aluminium alloys evaluated in this study. For each condition, three tensile tests were conducted. Table 7 presents the HCI index of laser welds as a function of the mechanical properties.

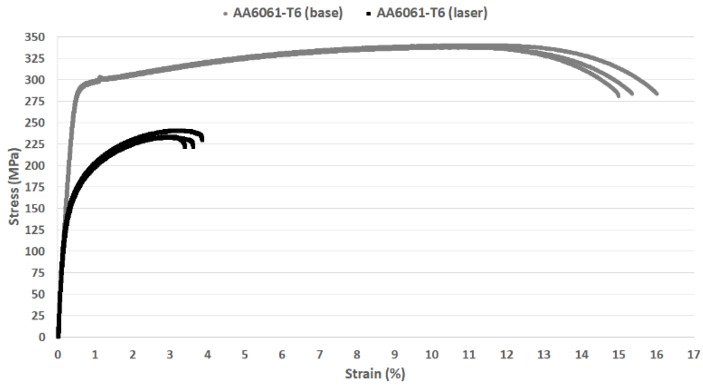

(**a**)

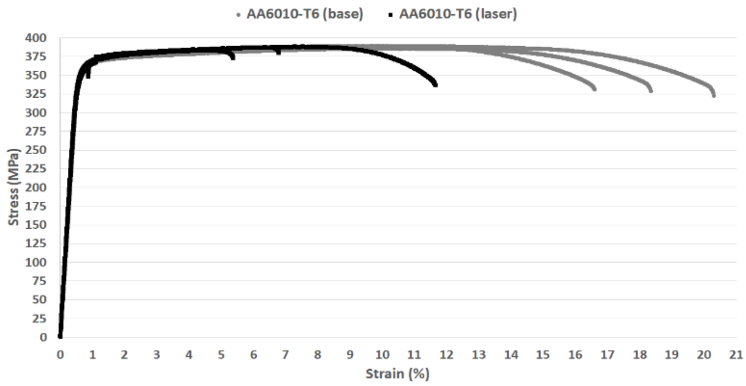

(**b**)

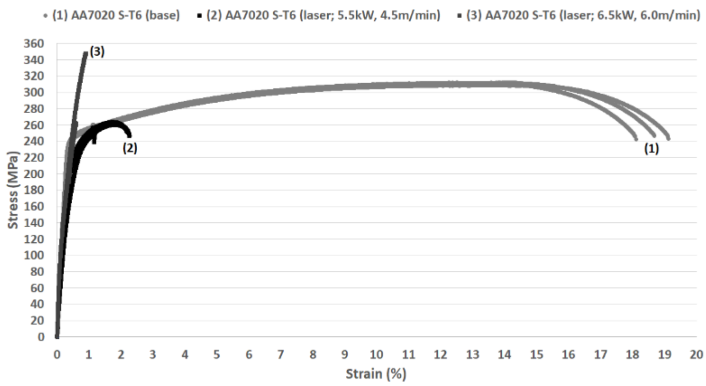

(**c**)

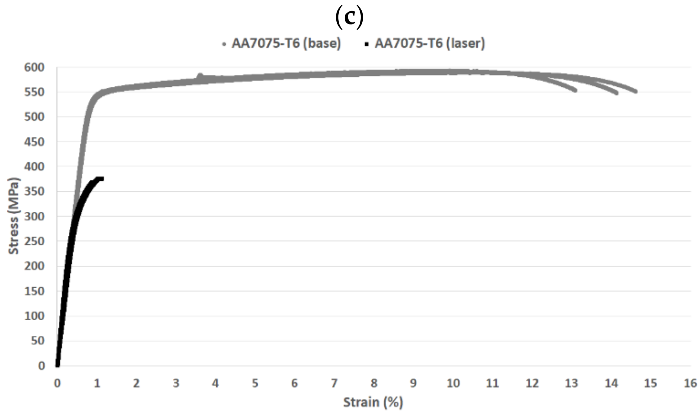

(**d**)

Figure 21. Mechanical tensile curves comparing different laser weld HCI indexes upon the various aluminium alloys: (**a**) AA6061-T6, 6.0 kW-6.5 m/min, HCI 0.23; (**b**) AA6010-T6, 6.0 kW-6.5 m/min, HCI 0.28; (**c**) AA70720 S-T6, 5.5 kW-4.5 m/min, HCI 0.24 and 6.5 kW-6.0 m/min, HCI 0.46; and (**d**) AA7075-T6, 6.0 kW-6.5 m/min, HCI 2.74.

Table 7. HCI index of laser welds as function of the mechanical properties.

Alloy	HCI Index	Yield Stress MPa	Ultimate Tensile Stress MPa	Elongation at Fracture %
AA6061	0.23	162.3 +/− 1.5	236.0 +/− 4.4	3.63 +/− 0.24
AA6010	0.28	356.7 +/− 2.9	386.5 +/− 2.5	7.93 +/− 3.29
AA7020 S	0.24	205.3 +/− 1.2	262.3 +/− 1.5	2.23 +/− 0.06
AA7020 S	0.46	201.3 +/− 16.3	244.3 +/− 114.2	0.58 +/− 0.34
AA7075	2.74	336.3 +/− 6.7	366.7 +/− 10.7	0.93 +/− 0.18

The elongation at fracture of AA6061-T6 and AA7075-T6 aluminium alloys was in the same range (respectively, 14.87% and 13.95%) while AA6010-T6 and AA7020 S-T6 exhibited higher values (respectively, 18.42% and 18.64%). From Figure 21, it can be seen that the laser welds showing a low HCI index ($\leq$0.3) have some degree of uniform elongation and the elongation at fracture values are also higher. The laser welds tested with a high HCI index (0.46 and 2.74) did not present any uniform elongation explained by the low elongation at fracture values reported (<1%). The HCI index is plotted against the elongation at fracture values of laser welds in Figure 22.

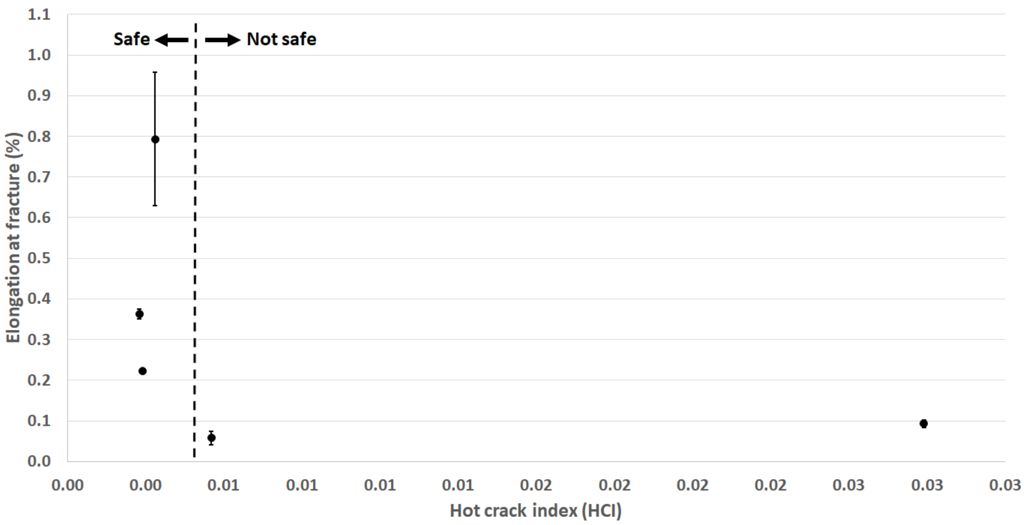

Figure 22. HCI index as function of the elongation at fracture values of laser welds.

Although the relationship is drawn over a small dataset (5), there is a clear indication that the number of hot cracks can play a role in the overall laser weld ductility in tensile loading. A HCI value ranging between 0.3 and 0.4, based on these results, appears to be an acceptable threshold limit toward a safe number of admissible hot cracks in laser welds of aluminium alloys to at least prevent a fragile tensile behavior. For AA6061 and AA7020 S aluminium laser welds showing elongation at fracture values $\geq$ 2.0%, the fracture zones were observed either at the fusion line or in the fusion zone (Figure 23).

This behavior was expected since laser welding was conducted on these aluminium alloys under a T6 metallurgical state, which indicates an overaged condition in the fusion and heat-affected zones. The AA7020 S and AA7075 aluminium laser welds that showed the lowest elongation at fracture values (<1%) exhibited the same tensile fracture locations (Figure 24), nonetheless, almost no necking is observed. The AA6010 laser welds had the highest elongation at fracture values (7.93%), which was considerably higher (two to four times) than for AA6061 and AA7020 S laser welds. These higher values were obtained because the processing route for AA6010 laser welds was considered a complete solution of heat and aging treatment after welding.

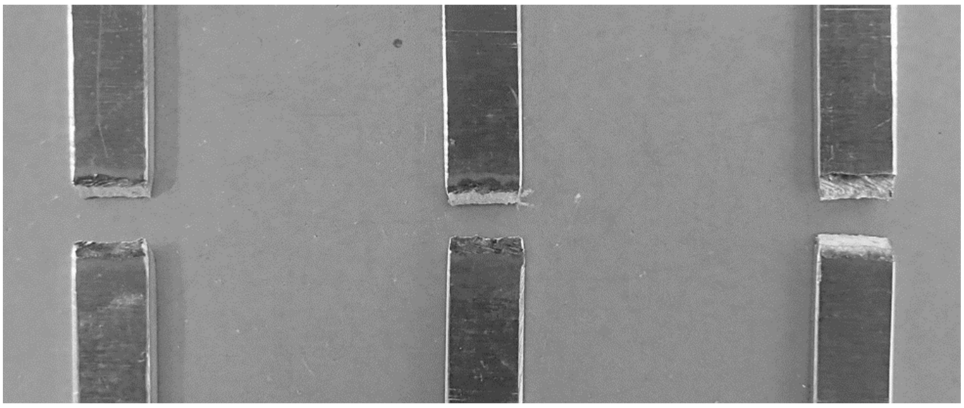

Figure 23. Tensile fracture locations of AA7020 S laser welds, HCI index 0.24.

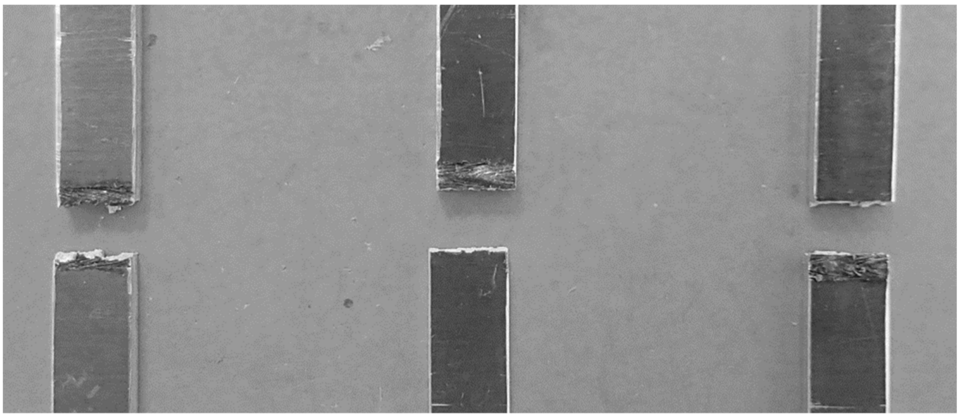

Figure 24. Tensile fracture locations of AA7020 S laser welds, HCI index 0.46.

The final weld metallurgical state is in T6 (peak aging), which maximizes the post-weld mechanical properties. The fracture location was observed in the heat-affected zone (HAZ) which probably indicates a different precipitation behavior between the HAZ and the fusion zone (Figure 25).

Figure 25. Tensile fracture locations of AA6010 laser welds, HCI index 0.28.

However, no conclusion can be stated about the effect of a post-weld complete solution heat and aging treatment (T6) depending on the HCI index as no tensile tests were conducted on such conditions where a high HCI index was obtained.

4. Conclusions

This work studied the effect of various aluminium alloys (AA6061, AA6010, AA7020 S, AA7075), and to some extent that of different process parameters, upon autogenous laser wobbling toward the hot cracking response. Laser welding, especially without the use of a filler wire, is gaining interest in automotive manufacturing for battery enclosure joining, but leak-tight components without cracking are expected. The hot cracks were characterized by optical microscopy and a hot crack index (HCI) was defined and related to the static mechanical properties. This study highlights:

- The HCI values of laser welds increase as function of the cracking susceptibility index (CSI) of the base material predicted using a thermodynamic CALPHAD-based software, PANDAT [16]. For lower CSI value (3–4), referring to AA6061 aluminium alloy in this study, a low HCI index (<0.25) was observed independently of the welding parameters. For higher CSI value (6–7), referring to AA7075, the behavior followed the same behavior as the HCI index was also high (>1.65). For intermediate values of CSI (4–5), related to AA6010 and AA7020 S aluminium alloys, the HCI values depended strongly on the welding parameters. If the laser power was kept <6.0 kW and the travel speed < 5.0 m/min, the HCI index remained low (<0.3). An increase in laser power and travel speed increased the HCI index gradually where a maximum value was reached (1.0).
- The hot cracks were divided into two main length classes: <500 μm and $\geq$500 μm. Every aluminium alloy that was welded (AA6061, AA6010, AA7020 S, AA7075) induced a higher number of long cracks compared to the small ones without regard to the HCI index value. It could be then stated that the hot cracking fundamentals appeared similar.
- The elongation at the fracture obtained in static tension was related to the extent of HCI. A threshold HCI value $\approx$ 0.3–0.4 was reasonable to ensure an elongation at fracture value >1%.

The effect of the hot crack index (HCI) as a function of the mechanical properties could be applied, in a follow-up of this study, to different load cases such as uniaxial fatigue or VDA bending tests.

Author Contributions: Methodology: F.N.; laser welding experiments: F.N. and F.M.; results and analysis: F.N.; revision: F.M. All authors have read and agreed to the published version of the manuscript.

Funding: This research was funded through the NRC METALTec industrial group. More specifically, a CQRDA research funding was attributed (CONT 1123) under the project name 'Soudage laser haute productivité 4.0′.

Institutional Review Board Statement: Not applicable.

Informed Consent Statement: Not applicable.

Data Availability Statement: The data provided in this paper cannot be accessible as they were provided under the NRC industrial group METALTec, although members acknowledge publishing.

Acknowledgments: NRC would like to acknowledge its METALTec industrial group members for material procurement (AA6010, AA7020 S).

Conflicts of Interest: The authors declare no conflict of interest.

References

1. The Aluminium Association. *Roadmap for Automotive Aluminium*; Drive Aluminium: Arlington, VA, USA, 2021; pp. 1–81.
2. Afseth, A. *Aluminium Battery Enclosure Design*; Center for Automotive Research—Constellium North America: Ann Arbor, MI, USA, 2021; pp. 1–28.
3. Hayashida, A.; Kakigi, T. Robust Design on Adhesive Material and Bonding Process for Automotive Battery Pack. In *WCX SAW World Congress Experience*; SAE International: Detroit, MI, USA, 2019; pp. 1–6.

4. Sabry, N.; Stroh, J.; Sediako, D. Characterization of microstructure and residual stress following the friction stir welding of dissimilar aluminium alloys. *CIRP J. Manuf. Sci. Technol.* **2023**, *41*, 365–379. [CrossRef]
5. Sokolov, M.; Franciosa, P.; Ceglarek, D. Remote laser welding of die casting aluminium parts for automotive applications with beam oscillation and adjustable ring mode laser. In Proceedings of the Lasers in Manufacturing Conference, Munich, Germany, 21–24 June 2021; pp. 1–11.
6. Mirakhorli, F. Trends in aluminium laser welding: Lightweight applications. In Proceedings of the CanWeld Conference, Montréal, QC, Canada, 13–14 September 2017; pp. 1–27.
7. Cross, C.E.; Coniglio, N. Weld Solidification Cracking: Critical Conditions for Crack Initiation and Growth. In *Hot Cracking Phenomena in Welds II*; Springer Nature: New York, NY, USA, 2008; pp. 47–66.
8. Cheng, C.M.; Chou, C.P.; Lee, I.K.; Lin, H.Y. Hot cracking of welds on heat treatable aluminium alloys. *Sci. Technol. Weld. Join.* **2005**, *10*, 344–352. [CrossRef]
9. Kah, P.; Hiltunen, E.; Martikainen, J. Investigation of Hot Cracking in the Welding of Aluminium Alloys (6005 & 6082). In Proceedings of the 63rd Annual Assembly & International Conference of the International Institute of Welding, Istanbul, Turkey, 11–16 July 2010; pp. 373–380.
10. Holzer, M.; Hoppe, F.; Mann, V.; Hofmann, K.; Hugger, F.; Roth, S.; Schmidt, M. Influence of filler wire and focus diameter on crack formation in laser beam welding of high-strength aluminium alloys. In Proceedings of the Lasers in Manufacturing Conference, Munich, Germany, 22–25 June 2015; pp. 1–11.
11. Holzer, M.; Hofmann, K.; Mann, V.; Hugger, F.; Roth, S.; Schmidt, M. Change of hot cracking susceptibility in welding of high-strength aluminium alloy AA7075. *Phys. Procedia* **2016**, *83*, 463–471. [CrossRef]
12. Hagenlocher, C.; Weller, D.; Weber, R.; Graf, T. Reduction of the hot cracking susceptibility of laser beam welds in AlMgSi alloys by increasing the number of grain boundaries. *Sci. Technol. Weld. Join.* **2019**, *24*, 313–319. [CrossRef]
13. Ramiarison, H.; Barka, N.; Mirakhorli, F.; Nadeau, F.; Pilcher, C. Parameter optimization for laser welding of dissimilar aluminium alloy: 5052-H32 and 6061-T6 considering wobbling technique. *Int. J. Adv. Manuf. Technol.* **2022**, *118*, 4195–4211. [CrossRef]
14. Pang, X.; Dai, J.; Chen, S.; Zhang, M. Microstructure and mechanical properties of fiber laser welding of aluminium alloy with beam oscillation. *Appl. Sci.* **2019**, *9*, 5096. [CrossRef]
15. Kerstens, N.F.H. Nd: YAG Laser Welding of AA7075 High Strength Aluminium. Ph.D. Thesis, Delft University of Technology, Delft, The Netherlands, 2002.
16. Zhang, F.; Liang, S.; Zhang, C.; Chen, S.; Lv, D.; Cao, W.; Kou, S. Prediction of Cracking Susceptibility of Commercial Aluminium Alloys during Solidification. *Metals* **2021**, *11*, 1479. [CrossRef]